



# Amorphous carbon at low densities: An *ab initio* study



Bishal Bhattarai, D.A. Drabold\*

Department of Physics and Astronomy, Ohio University, Athens, OH 45701, USA

## ARTICLE INFO

### Article history:

Received 29 September 2016

Received in revised form

4 January 2017

Accepted 10 January 2017

Available online 12 January 2017

### Keywords:

*Ab initio*

Low density

Amorphous carbon

Phonons

Specific heat

## ABSTRACT

In this paper, we present new computer models of low-density amorphous carbon, and study the structural, electronic and vibrational properties all based upon plane-wave density functional methods. The static structure factor and real space pair-correlation function is in agreement with available experimental data. We observe chains of  $sp$  bonded carbon in the models, along with  $sp^2$  and  $sp^3$  structures in varying concentrations. These models provide atomistic insight into the microstructure of the system, delineating variation in bonding ( $sp^2$ ,  $sp^3$  and  $sp$ ) preferences as a function of density. For these low densities, the vibrational density of states is computed for the first time, along with localization of modes and the specific heat with comparison to experiments. We contrast the amorphous three dimensional networks with amorphous graphene, which bears a striking similarity in the radial distribution functions, but shows a distinct signature in the vibrational density of states. The vibrational modes are analyzed and discussed, and animations of particularly interesting modes are provided as Supplementary Material. The modes are generally well extended, but are more complex than simple molecular pictures that are sometimes invoked, in some cases even revealing mixing among modes of different type.

© 2017 Elsevier Ltd. All rights reserved.

## 1. Introduction

Amorphous carbon has been an important research topic both for its many technological applications, and its scientific interest due to its remarkable ability to form an array of microstructures. Carbon forms bonds of  $sp$ ,  $sp^2$  and  $sp^3$  type [1], and these tend to be surprisingly energy-degenerate. An interesting question we will explore is the concentration of these three types of bonds as a function of density. Experimentally, non-hydrogenated amorphous carbons are challenging [2], which further justifies a new theoretical study. The variation in low density carbon samples arise in part from the method of preparation of the sample and the heat-treatment [3]. Furthermore, glassy carbon may be extracted from various polymers, which may leave a residue of bonded H. The presence of hydrogen significantly impacts the inelastic neutron scattering spectrum [4].

Some earlier research on amorphous carbon was been focused on tetrahedral (ta-c) or diamond-like carbon [5,6], along with amorphous graphene [7] and its applications. ta-C was explored

mostly in the hope of devising a dopable substitute for diamond for electronic applications. To date, there have been few modeling studies of low-density ( $1.0 - 1.5 \text{ g/cm}^3$ ) amorphous carbon phases [8–10]. Such calculations are based on MD simulations, albeit with tight-binding [11], and Reverse Monte Carlo (RMC), respectively. An alternative scheme for modeling amorphous carbon, more reliable than RMC, is to use experimental information and a force field, along the lines of Opletal and coworkers [12] and in more recent related approaches [13–16].

In this paper, we present new models for low density carbon. We have used state of the art *ab initio* interactions for our calculations. This approach provides a benchmark, as we obtain the atomistic models without any *a priori* assumptions of the system and accurate interatomic forces. Further, this paper will be an extension of the previous *ab initio* method based theoretical work done for higher densities of amorphous carbon [17].

The paper is organized as follows, In section 2 we discuss the computational methodology. In section 3, we report our models and the methods of preparation. Section 4, mainly focuses on the structural properties of the models and comparisons to experiments. Section 5 is devoted to the vibrational properties of the system, localization, identification of the vibrational states and the low-temperature specific heat. Section 7 gives a brief description of electronic properties of these low density carbons by evaluation the

\* Corresponding author.

E-mail addresses: [bb248213@ohio.edu](mailto:bb248213@ohio.edu) (B. Bhattarai), [drabold@ohio.edu](mailto:drabold@ohio.edu) (D.A. Drabold).

**Table 1**

Nomenclature and details of our models: density of the models ( $\rho$ ), position of first ( $r_1$ ) and second ( $r_2$ ) peak of RDF, Mean co-ordination number ( $n$ ), percentage of  $sp^3$ ,  $sp^2$  and  $sp$ , cooling time/cooling rate and the Free Energy per atom of the relaxed models ( $E_0$ ).

Model	$\rho$ (g/cm <sup>3</sup> )	$r_1$ (Å)	$r_2$ (Å)	$n$	% of $sp^3$	% of $sp^2$	% of $sp$	cooling time (ps)/rate (K/ps) <sup>a</sup>	$E_0$ (eV/atom) <sup>b</sup>
c64_4ps	1.50	1.43	2.45	2.90	6.25	78.12	15.63	4.0/1850.0	0.13
c120_15ps	1.50	1.45	2.49	2.90	4.17	81.67	14.16	15.0/493.3	0.15
c120_20ps	1.50	1.44	2.48	2.93	9.17	75.00	15.83	20.0/370.0	0.11
c72_16ps	0.92	1.41	2.48	2.67	0.00	66.67	33.33	16.0/462.5	0.35
c72_20ps	1.40	1.43	2.46	2.89	7.00	75.00	18.00	20.0/370.0	0.00
c72_20ps <sup>†</sup>	1.60	1.43	2.47	2.86	4.17	77.78	18.05	20.0/370.0	0.02

<sup>a</sup> Refers to cooling time or cooling rate from 8000 K to 600 K.

<sup>b</sup> After subtraction from lowest value of  $E_0$ .

electronic density of states and the electronic localization. In section 6, we summarize our findings and discuss the effectiveness of our approach by comparing it to the other known results. In section 8, we also describe animations of representative vibrational modes of interest.

## 2. Computational methodology

We have prepared models of glassy carbon [18] with densities ranging from (0.923 g/cm<sup>3</sup>–1.6 g/cm<sup>3</sup>). The models were prepared by using the *ab initio* Package “Vienna *Ab initio* Simulation Package” (VASP), a molecular dynamics package with a plane-wave basis and using the local-density approximation. The electron-ion interactions for the plane wave basis or VASP models were described by the Projector Augmented-Wave (PAW) [19,20] method with Ceperley-Alder exchange correlation functional. A liquid phase at each density was equilibrated and then “cooled” as described below yielding an arrested solid phase, which was then fully relaxed using the conjugate gradient (CG) method. All simulations were performed at constant volume, employing only the  $\Gamma(\vec{k} = 0)$  point to compute the forces and total energies.

## 3. Models

We have prepared models with system size ranging from 64 atoms to 120 atoms.<sup>1</sup> We have chosen densities varying between (0.923 g/cm<sup>3</sup> - 1.6 g/cm<sup>3</sup>). We began with random coordinates, these were “heated” to 8000 K, equilibrated at 8000 K and then cooled to 300 K in multiple steps (see Table 1). Finally, a well-equilibrated model at 300 K was relaxed using the conjugate gradient (CG) scheme.

The resulting six models provide us with a reasonable selection of low density regime in amorphous carbon. These models will hereafter be identified as (c64\_4ps, c120\_15ps, c120\_20ps, c72\_16ps, c72\_20ps and c72\_20ps<sup>†</sup>). These assigned nomenclatures indicate: the number of atoms in the cell, and the cooling time used for each model. We summarize our models in Table 1.

## 4. Structural properties

A visual representation of these models has been provided in Figs. 1 and 2. We have used periodic boundary conditions to replicate the (c120\_15ps) model and show 720 atoms in Fig. 1. Meanwhile, in Fig. 2, the various bonding environments have been assigned different colors. These reveal that  $sp^3$  bonding mainly inter-connects the  $sp^2$  bonding networks and that  $sp^2$  bonding

dominates for lower density. Interestingly, a significant fraction of  $sp$  bonded atoms are also formed in low density carbon, providing a chain-like topology, familiar from a-Se [22]. In particular, our model (c72\_16ps) at a density of 0.923 g/cm<sup>3</sup> has 33%  $sp$  bonded atoms. To our surprise this model has the same final free energy per atom ( $E_0$ ), as the other model with much less  $sp$  content, which suggests that at low concentration the  $sp$  bonding is to be expected [23] and justifies the common assertion that the three hybridizations yield similar local energetics. The  $sp$  bonded model is shown in Fig. 2. These  $sp$  chains were first conjectured in the work of McCulloch et al., we show that their conclusions were valid. We have also compared our results (see Fig. 3) with the amorphous graphene network [24]. To our surprise, despite the fact that our amorphous carbon is three dimensional in nature (see Fig. 1), structurally it resembles strictly the two dimensional amorphous graphene (albeit puckered around pentagonal structures) [7].

The structure of low density carbon has been controversial as different heat treatment protocols yields different structural features [10]. Further, there has also been a debate about the bonding present in these structures. Mildner and Carpenter [3] suggested that the concentration of  $sp^3$  bonding in these materials is less than 10 %. Our models are in agreement with this claim, as all of our models have  $sp^3$  fraction below 10 %.

Structurally, glassy carbon can be described with the help of the Static Structure Factor in reciprocal space or its real space counterpart the Radial Distribution function (RDF). The RDF obtained for the models are plotted in Fig. 3 and also for a model of amorphous graphene. The position of the first and second peak from the RDF is similar for the different models irrespective of the different carbon bonding environments and the method used for making the models. The peak positions and the coordination number are in good agreement with previous calculations [8,10,26] and with

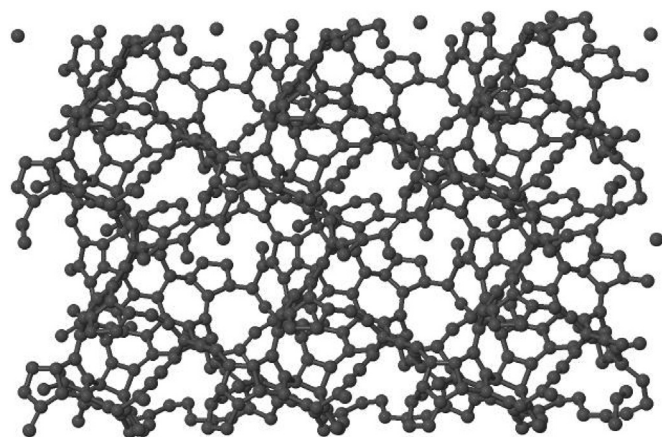


**Fig. 1.** Visualization of model (c120\_15ps), 720 atoms are shown (replicated by using periodic boundary condition).

<sup>1</sup> We also prepared a larger model (with 216 atoms) using SIESTA [21], with (Harris Functional). The non-self consistent scheme resulted in slightly larger fraction of  $sp^3$  and a minor shift in RDF was observed, with almost no change in other properties.

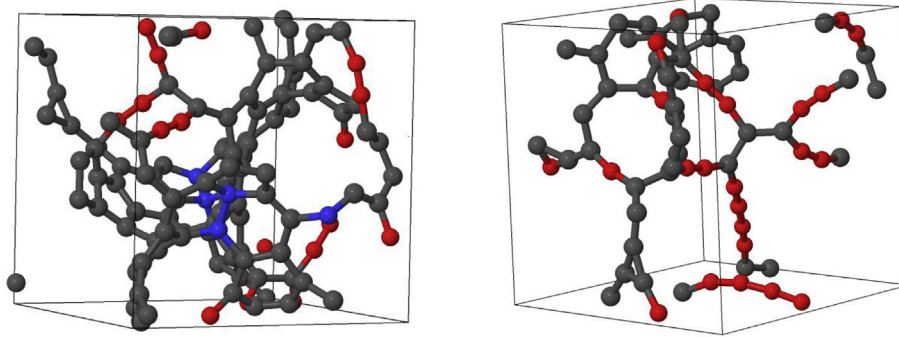


**Fig. 2.** Visualization of the different bonding: grey ( $sp^2$ ), blue ( $sp^3$ ) and red ( $sp$ ). (**Left Panel**): c120\_15ps,  $\rho = 1.50\text{g/cm}^3$  and (**Right Panel**): c72\_16ps,  $\rho = 0.923\text{g/cm}^3$ . (A colour version of this figure can be viewed online.) Periodic boundary conditions were used, only atoms in the reference cell are shown.

experiments [3].

Comparison of experiment and theory for the structure factor and the radial distribution function (RDF) are given in Fig. 3. Firstly, we compare the obtained structure factor with the experimental data for amorphous carbon at a density ( $\rho = 2.0\text{g/cm}^3$ ) [25]. Similarly, Fig. 3 shows another comparison of experimental data obtained for the glassy carbon at a density ( $\rho = 1.55\text{g/cm}^3$ ) [10], with the radial distribution function. Experimentally, the first three peaks of the RDF for glassy carbon are at distances, 1.42 Å, 2.46 Å and 3.75 Å. There is pleasing agreement with these observations. Additionally, there are peaks or shoulders occurring at distances, 2.84 Å, 4.27 Å and so on [3,10,27]. As seen in Fig. 3, there is a narrow shoulder at distance ( $\sim 1.10$  Å) in the experimental RDF [10] and it is also seen in the TBMD simulation [8] (especially for the low density models). This narrow shoulder is not seen in our models. From Table 1, it should be noted that different cooling temperatures for the simulation results in slight difference in the fraction of ( $sp^2$ ,  $sp^3$  and  $sp$ ) bonds with little or no effect on the RDF and peak positions.

#### 4.1. Angle distribution functions

The coordination numbers (listed in Table 1), are dominated by trigonal for low density carbons. This indicates that the carbon-carbon angle distribution is likely to peak near  $120^\circ$ . Several models and experiments indicate a slightly different value of the bond angles for these carbon. Beeman et al. [26] calculated the angle distribution for classic handmade models and found these angles slightly less than expected  $\sim 117.7^\circ$  for the three

coordinated models.

The angle distribution functions for the models are plotted in Fig. 4. The peaks are in harmony with the our assumptions except for the model (c72\_16ps). In this model the presence of a high percentage of  $sp$  bonds results in a broader distribution of the peaks. Further, a tiny (and probably physically meaningless) fraction of bond angles are seen at  $\sim 50^\circ$ .

#### 4.2. Ring distribution

The ring distribution provides us with more information about the connectivity of the networks. The ring statistics are shown in Fig. 4 and were obtained by King's shortest path [28] scheme, using the ISAACS [29] program. The ring statistics thus obtained have a broad distribution of with the maximum of most models peaking at 5-membered-rings as opposed to 6-membered-rings for graphite [17]. The results of ring statistics obtained here (albeit with interconnecting  $sp$ -chains) are consistent with the previous results [10,17]. The connectivity of the high  $sp$  model (c72\_16ps) has a slight different characteristics as, a few rings are observed with high number of nodes.

### 5. Vibrational properties

#### 5.1. Computing the dynamical matrix

The dynamical matrix was obtained by displacing each atom in 6-directions ( $\pm x, \pm y, \pm z$ ) by a small displacement of 0.015 Å. Then,

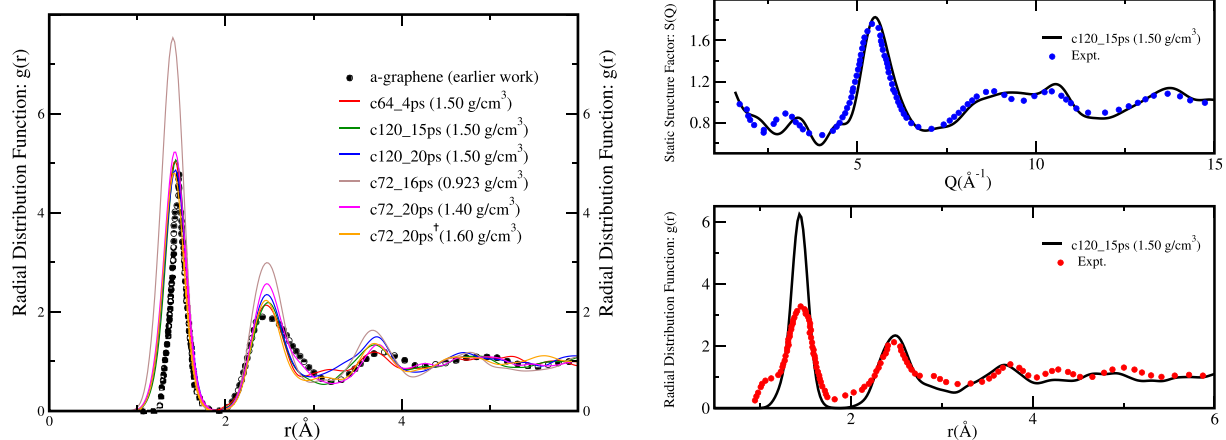


**Fig. 3.** (**Left panel**) Radial distribution function for the different models (solid lines) and comparison with the amorphous graphene [24]. (**Right panel**) (top) Static structure factor for the model (c120\_15ps) (black, solid line) versus experimental structural factor data of amorphous carbon ( $\rho = 2.0\text{g/cm}^3$ ) [25] (blue, solid circles), (bottom) RDF for the model (c120\_15ps) (black, solid line) versus experimental RDF for density ( $\rho = 1.55\text{g/cm}^3$ ) [10]. (A colour version of this figure can be viewed online.)

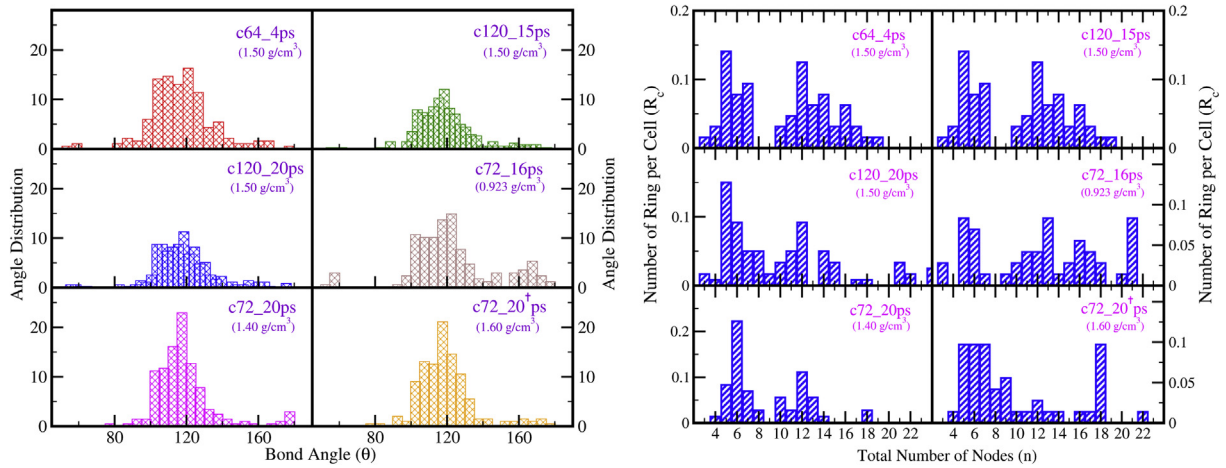


Fig. 4. (Left panel) Bond-angle distribution function for the models, (Right panel) Ring distribution for the models [28,29]. (A colour version of this figure can be viewed online.)

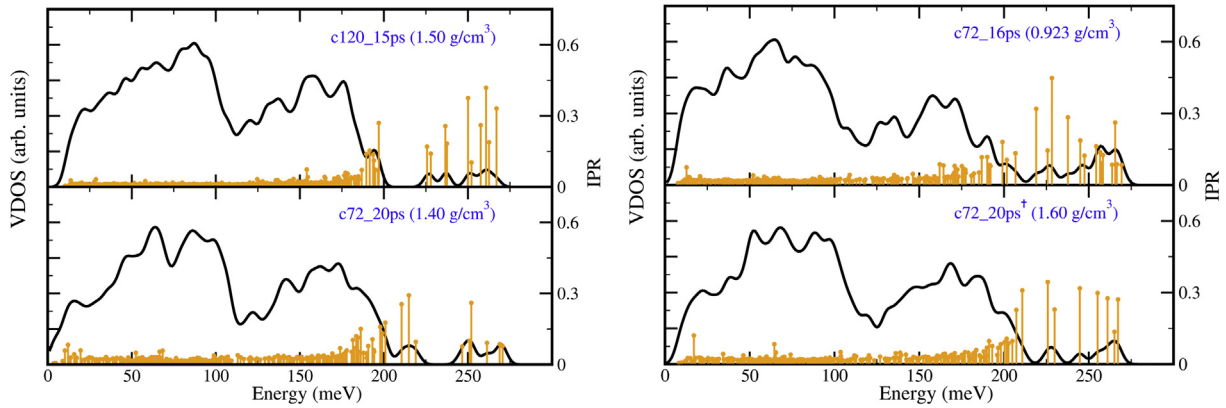


Fig. 5. Vibrational Density of States (VDOS) at four different densities (black, solid line), The Inverse Participation Ratio (IPR) describes the localization of the modes (orange, drop lines) (see Eq. (1)), larger IPR implies more compact modes. (A colour version of this figure can be viewed online.)

*ab initio* force calculations were performed to obtain the force constant matrix. The details of the force constant matrix calculation is provided elsewhere [30,31]. We have Gaussian broadened the eigenvalues (using a width  $\sigma \sim 3.0$  meV) to obtain the VDOS. The first three  $\omega = 0$  frequencies (arising from rigid cell translations) have been ignored for both the VDOS and the vibrational IPR.

Although we obtained the VDOS for the six models only four VDOS is plotted in Fig. 5. The other two VDOS for models (c64\_4ps and c120\_20ps) at density  $1.50\text{g/cm}^3$  are very similar to model (c120\_15ps) with density  $1.50\text{g/cm}^3$ . In spite of their differences, the VDOS obtained have a similar character for example, models below ( $\sim 200$  meV) are well extended modes. Further, despite the fact that the densities of these four models vary from ( $1.6\text{g/cm}^3$  to  $0.923\text{g/cm}^3$ ), we didn't obtain any low energy localized modes as seen in calculations with voids for a-Si [32]. Additionally, we show a comparison of the plot between the VDOS obtained for a-graphene [7] and our model (c72\_20ps,  $1.40\text{g/cm}^3$ ) in Fig. 6. The plots have bear considerable similarity, excepting the an intense peak near 80 meV. The band between about 110 meV and 200 meV is strikingly similar for amorphous graphene and our  $1.40\text{g/cm}^3$  model. The intense peak could perhaps be used as a diagnostic for the presence of amorphous graphene.

### 5.2. Vibrational localization

We can evaluate the localization (the spatial extent of the

normal modes) by defining the inverse participation ratio (IPR),  $\mathcal{I}$ . The IPR can be easily calculated from normalized displacement vectors [31], IPR for the vibrations can be defined as,

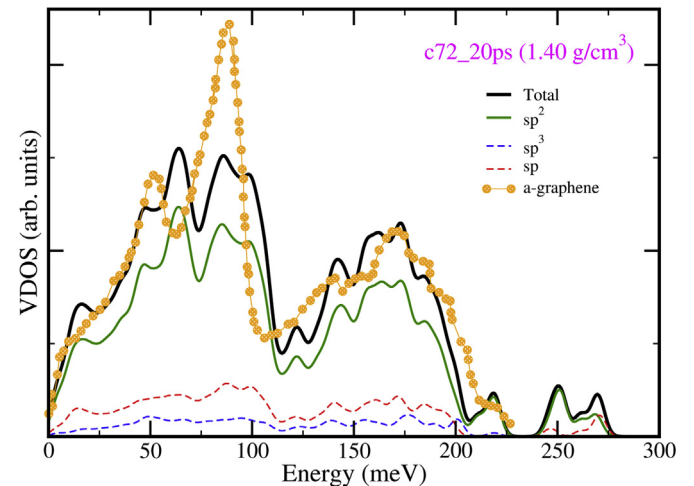


Fig. 6. Vibrational density of states of model (c72\_20ps,  $1.40\text{g/cm}^3$ ) compared with amorphous graphene [7]. (A colour version of this figure can be viewed online.)

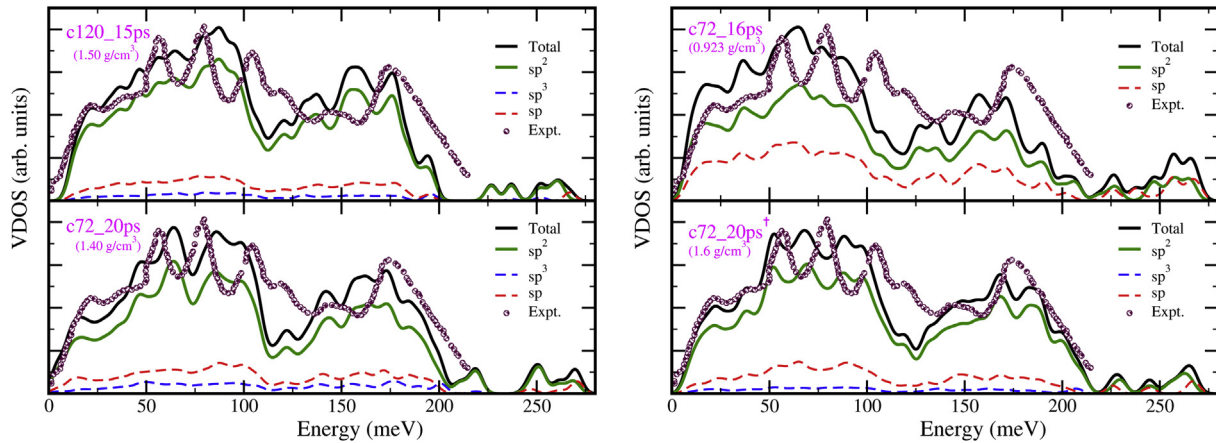


Fig. 7. Plot showing Total VDOS, ( $sp^3, sp^2, sp$ ) projected VDOS and the experimental results [34] for glassy carbon. (A colour version of this figure can be viewed online.)

$$\mathcal{I} = \frac{\sum_{i=1}^N |u_i^j|^4}{\left(\sum_{i=1}^N |u_i^j|^2\right)^2} \quad (1)$$

The inverse participation ratio of a localized displacement is  $\mathcal{I} \approx 1$  and the extended or de-localized displacement is  $\sim 1/N$ . The IPR is shown alongside the VDOS in Fig. 5. The localized modes are mostly concentrated high frequency. The localized modes involve the motion of very few atoms and these high frequencies modes are most likely to be of stretching character.

### 5.3. $sp - sp^2 - sp^3$ projected VDOS

In our previous calculations [31], we presented the details for computing the species-projected VDOS. Here, we computed the VDOS contributions due to the different bonding ( $sp - sp^2 - sp^3$ ) for the 4 models with different densities. This projection gives further insight to the different contribution to the vibration among the bonding units. These projected VDOS are plotted in Fig. 7. As expected, the  $sp^2$  contribution to the VDOS is the most significant [33], and makes contributions to all the major peaks in the VDOS. The  $sp^3$  and  $sp$  contributions largely perturb the peaks originating primarily from the  $sp^2$ -associated modes. At higher energy ( $\sim 200$  meV or more), the contributions are mostly from  $sp$  and  $sp^2$  modes, as one might expect from the strength of these carbon bonds.

We have also compared with the experimental results of Kamitakahara et al. [34] for the glassy carbon (see Fig. 7). We observe qualitative agreement with the experimental results. Our VDOS matches the experimental results at the lower energy regime ( $\sim 50$  meV), while some discrepancies are seen at higher frequencies. We have previously shown [31] in our work on  $a\text{-SiO}_2$ , that an accurate potential and the system size greatly affects the VDOS to obtain well defined resolution of the notable peaks.

### 5.4. $sp - sp^2 - sp^3$ projected IPR

We also investigate the contribution to the localization due to each type of bonding environments with our system. It is not surprising to see that the most localized modes arise from  $sp$  and  $sp^3$  bonding. The results of the projected IPR is presented in Fig. 8. Where, the model with the least  $sp^3$  bonding [present in an amount of ( $< 10\%$ )] has the most localized modes. Meanwhile,  $sp$  bonding yields fairly extended modes for the lower regime ( $< 200$  meV), while there are few significant localized modes on the optical regime. This also suggests that a few percent of  $sp$  modes in these low density carbons are expected.

### 5.5. Specific heat

The specific heat in the harmonic approximation is easily obtained from the density of states,  $g(\omega)$ . We note that for

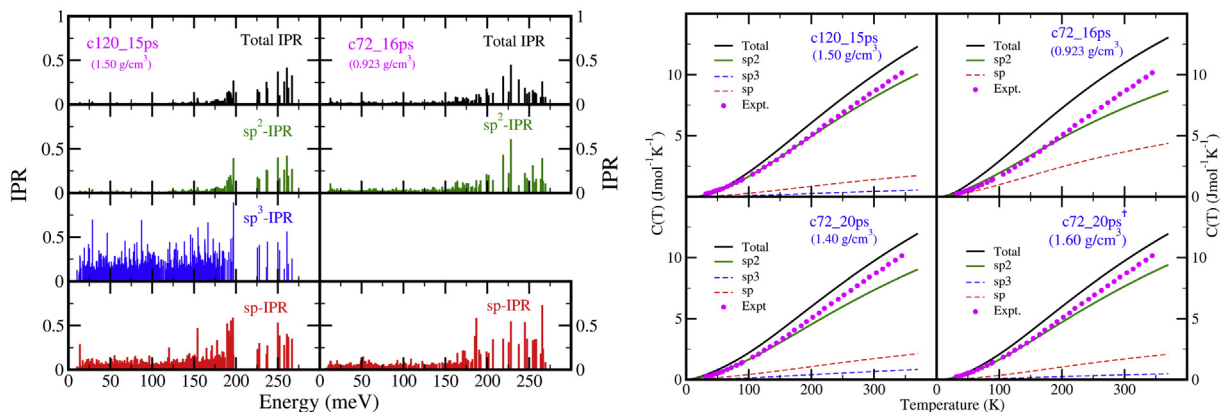
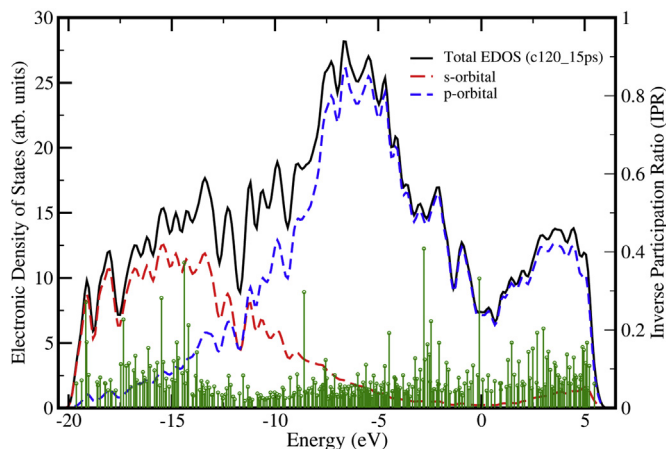


Fig. 8. (Left Panel:) Plot of ( $sp^3, sp^2, sp$ ) projected IPR along with the Total IPR for the obtained models, (Right Panel:) Low temperature dependence of specific heat for the four models versus the experimental results [35], (A colour version of this figure can be viewed online.)



**Fig. 9.** Plot of EDOS ( $E_F = 0$ ) for the c120-a model: (black, Total EDOS), (red-dashed, s-orbital EDOS), (blue-dashed, p-orbital EDOS), the localization (green-drop lines, IPR). (A colour version of this figure can be viewed online.)

wavelengths larger than our supercell size, modes are suppressed and are not included in the obtained VDOS. We compute the specific heat  $C_V(T)$  from the relation [32,36],

$$C(T) = 3R \int_0^{E_{\max}} \left( \frac{E}{k_B T} \right)^2 \frac{e^{E/k_B T}}{(e^{E/k_B T} - 1)^2} g(E) dE \quad (2)$$

Here, the VDOS ( $g(E)$ ) is normalized to unity.

In Fig. 8, we see that  $C_V(T)$  for our four models is in reasonable agreement with experiment. Glassy carbon has a higher value of specific heat and lower density than graphite [35]. These facts are manifested by our models. Inferring from Fig. 8, the model (c72\_16ps) (Fig. 8) which has the lowest densities ( $0.923 \text{ g/cm}^3$ ) among the models has a higher value of specific heat compared to the other models.

Similar to the ( $sp - sp^2 - sp^3$ ) projected VDOS, we have computed the specific heat due to partial contribution of different bonding environments. The results due to this decomposition leads to an interesting result. We observe that the contribution due to the partial- $sp^2$  VDOS in the low temperature specific heat matches quite well with the experimental result [35]. It must be noted that

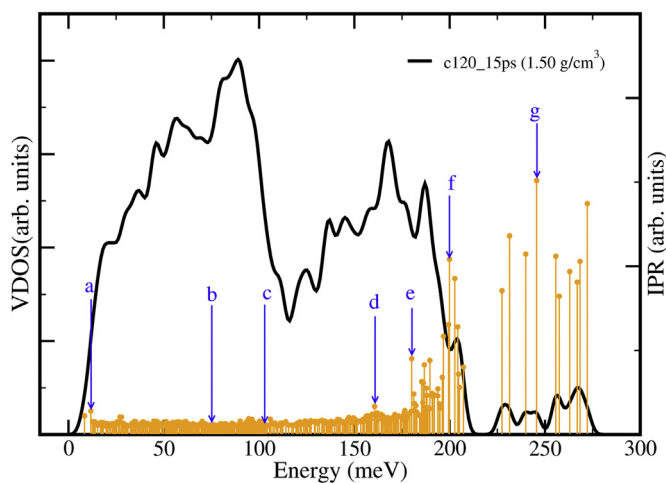


**Fig. 10.** Vibrational Density of States (VDOS) (black, solid line) and Inverse Participation Ratio (IPR) (orange, drop lines) at density  $1.50 \text{ g/cm}^3$ . The letters depict modes for which animations are given in the Supplementary material. (A colour version of this figure can be viewed online.)

the  $sp$  bonding has a significant effect on the total specific heat obtained for the models, while the contributions from the  $sp^3$  bonding remains minimal. We have also verified the “3R-limit” (Dulong-Petit) limit at high temperature for our models (not shown here). To the extent that the hybridization-projected specific heat functions are well-defined and distinct, it may prove possible to use the T-dependence of the specific heat to estimate the concentration of  $sp$ ,  $sp^2$  and  $sp^3$  sites in a sample. More work is needed to see if this could be practical.

## 6. Electronic density of states

The concentration of  $sp$ ,  $sp^2$  and  $sp^3$  states is determined by the density [17]. The electronic density of states (EDOS) is strongly impacted by these different electronic hybridizations. The EDOS plot of one representative model is shown in Fig. 9. Our EDOS is in agreement with earlier research [17,37]. In Fig. 9, we show that the p-orbital contribution is more significant near the conduction edge. The electronic localization (IPR) [38] shows that at these lower densities these amorphous carbon are conductive (with a large density of extended states near the Fermi level) as expected [17]. This pattern of EDOS is consistent through out our other models without any significant differences, other than different weightings arising from the various hybridizations present for different densities.

## 7. Conclusions

We found that our *ab initio* based models reproduce most of the properties of the low density amorphous carbon, while improving upon some of the previous calculations and drawing comparisons to amorphous graphene. At these low densities, amorphous carbon consists of a mixed network involving  $sp^2$ ,  $sp^3$  bonds as expected and at the lowest densities a non-negligible contribution from  $sp$  bonds.

We have predicted that the vibrational contribution of the  $sp^2$  bonding is the most significant and it governs the total vibrations in these materials. Further, we also show that these  $sp^2$  guided vibrations are extended and evenly distributed. We note that the vibrational modes are more complex and non-local than simple molecular models would suggest. While such models certainly capture some of the basic character of the vibrations, the real modes are delocalized and sometimes mix with other nearby resonant modes. We believe that there is both scientific and pedagogic values in the animations that we provide from this work. We also note similarities and differences between a-C and hypothetical amorphous graphene materials.

## 8. Supplementary materials

A visual description of several interesting modes, along with the intermixing of different modes gives us a vivid picture of this vibrations on an atomic scale [39]. We used the same techniques as our earlier work [31] to reproduce some of the interesting modes (see Fig. 10). In particular, model (c120\_15ps) strike us an interesting model for this visual study. We relaxed our model using the *ab initio* software SIESTA [21], with a double- $\zeta$  basis and performed a force calculation to obtain the animations [40]. These animations highlights mixing of different vibrational motions (bending, rocking, stretching), suggesting that the vibrational motions on atomic scale is complex in nature for disordered solids.

- (a) 12 meV, this mode is particularly interesting as the whole block of carbon atoms move thus preserving the bond lengths at this low energy.

- (b) 75 meV and (c) 103 meV, we see a mixing of different vibrations at these frequencies.
- (d) 161 meV, it represents another well extended region of vibrational motion, where we see that stretching motion starts dominates over (bending, rocking, etc.) motions.
- (e) 179 meV, (f) 199 meV and (g) 245 meV, in these modes we look at few localized modes. These modes involve motion of fewer atoms compared to an extended mode. Further, the stretching motion dominates at these higher energies.

Supplementary video related to this article can be found at <http://dx.doi.org/10.1016/j.carbon.2017.01.031>.

## Acknowledgment

The authors would like to thank Dr. R.L. Cappelletti for many useful conversations and motivating this work. We also thank Prof. S. R. Elliott for comments. The authors are thankful to the NSF under grant number DMR 1507670. We acknowledge computing time provided by the Ohio Supercomputer Center.

## References

- [1] A.C. Ferrari, J. Robertson, Interpretation of Raman spectra of disordered and amorphous carbon, *Phys. Rev. B* 61 (2000) 14095–14107.
- [2] P. Mitchell, S. Parker, A. Ramirez-Cuesta, J. Tomkinson, *Non-hydrogenous Materials and Carbon*, vol. 3, World Scientific, Singapore, 2005, p. 487.
- [3] D. Mildner, J. Carpenter, On the short range atomic structure of non-crystalline carbon, *J. Non-Cryst. Solids* 47 (1982) 391–402.
- [4] P. Mitchell, S. Parker, A. Ramirez-Cuesta, J. Tomkinson, *Non-hydrogenous Materials and Carbon*, vol. 3, World Scientific, Singapore, 2005, p. 507.
- [5] D.A. Drabold, P.A. Fedders, M.P. Grumbach, Gap formation and defect states in tetrahedral amorphous carbon, *Phys. Rev. B* 54 (1996) 5480–5484.
- [6] J. Dong, D.A. Drabold, Ring formation and the structural and electronic properties of tetrahedral amorphous carbon surfaces, *Phys. Rev. B* 57 (1998) 15591–15598.
- [7] Y. Li, D.A. Drabold, Symmetry breaking and low energy conformational fluctuations in amorphous graphene, *Phys. Status Solidi B* 250 (2013) 1012–1019.
- [8] C. Wang, S. Qiu, K. Ho, O(n) tight-binding molecular dynamics study of amorphous carbon, *Comput. Mater. Sci.* 7 (1997) 315–323.
- [9] T. Frauenheim, G. Jungnickel, T. Köhler, U. Stephan, Structure and electronic properties of amorphous carbon: from semimetallic to insulating behaviour, *J. Non-Cryst. Solids* 182 (1) (1995) 186–197.
- [10] B. O'Malley, I. Snook, D. McCulloch, Reverse monte carlo analysis of the structure of glassy carbon using electron-microscopy data, *Phys. Rev. B* 57 (1998) 14148–14157.
- [11] C. Mathioudakis, G. Kopidakis, P.C. Kelires, C.Z. Wang, K.M. Ho, Physical trends in amorphous carbon: a tight-binding molecular-dynamics study, *Phys. Rev. B* 70 (2004), 125202(1–10).
- [12] G. Opletal, T.C. Petersen, D.G. McCulloch, I.K. Snook, I. Yarovsky, The structure of disordered carbon solids studied using a hybrid reverse monte carlo algorithm, *J. Phys. Condens. Matter* 17 (2005) 2605–2616.
- [13] K. Prasai, P. Biswas, D.A. Drabold, Electronically designed amorphous carbon and silicon, *Phys. Status Solidi A* 213 (2016) 1653–1660.
- [14] K. Prasai, P. Biswas, D.A. Drabold, Sculpting the band gap: a computational approach, *Sci. Rep.* 5 (2015), 15522(1–6).
- [15] A. Pandey, P. Biswas, D.A. Drabold, Force-enhanced atomic refinement: structural modeling with interatomic forces in a reverse monte carlo approach applied to amorphous Si and SiO<sub>2</sub>, *Phys. Rev. B* 92 (2015), 155205(1–8).
- [16] A. Pandey, P. Biswas, D.A. Drabold, Inversion of diffraction data for amorphous materials, *Sci. Rep.* 6 (2016), 33731(1–8).
- [17] D.G. McCulloch, D. McKenzie, C. Goringe, Ab initio simulations of the structure of amorphous carbon, *Phys. Rev. B* 61 (2000) 2349–2355.
- [18] G. Galli, R. Martin, R. Car, M. Parrinello, Ab initio calculation of properties of carbon in the amorphous and liquid states, *Phys. Rev. B* 42 (1990) 7470–7482.
- [19] G. Kresse, D. Joubert, From ultrasoft pseudopotentials to the projector augmented-wave method, *Phys. Rev. B* 59 (1999) 1758–1775.
- [20] P.E. Blochl, Projector augmented-wave method, *Phys. Rev. B* 50 (1994) 17953–17979.
- [21] J.M. Soler, E. Artacho, J.D. Gale, A. Garcia, J. Junquera, P. Ordejon, D. Sanchez-Portal, The siesta method for ab initio order-n materials simulation, *J. Phys. Condens. Matter* 14 (2002) 2745–2779.
- [22] X. Zhang, D.A. Drabold, Direct molecular dynamic simulation of light-induced structural change in amorphous selenium, *Phys. Rev. Lett.* 83 (1999) 5042–5045.
- [23] L. Ravagnan, F. Siviero, C. Lenardi, P. Piseri, E. Barborini, P. Milani, C.S. Casari, A.L. Bassi, C.E. Bottani, Cluster-beam deposition and in situ characterization of carbyne-rich carbon films, *Phys. Rev. Lett.* 89 (2002), 285506(1–4).
- [24] V. Kapko, D.A. Drabold, M.F. Thorpe, Electronic structure of a realistic model of amorphous graphene, *Phys. Status Solidi B* 247 (2010) 1197–1200.
- [25] F. Li, J. Lannin, Radial distribution function of amorphous carbon, *Phys. Rev. Lett.* 65 (1990) 1905–1908.
- [26] D. Beeman, J. Silverman, R. Lynds, M.R. Anderson, Modeling studies of amorphous carbon, *Phys. Rev. B* 30 (1984) 870–875.
- [27] S.F. Parker, S. Imberti, S. Callear, P. Albers, Structural and spectroscopic studies of a commercial glassy carbon, *Chem. Phys.* 427 (2013) 44–48.
- [28] S. King, Ring configurations in a random network model of vitreous silica, *Nature* 213 (1967) 1112–1113.
- [29] S. Roux, V. Petkov, ISAACS interactive structure analysis of amorphous and crystalline systems, *J. Appl. Cryst.* 43 (2010) 181–185.
- [30] M. Cobb, D.A. Drabold, R.L. Cappelletti, Ab initio molecular-dynamics study of the structural, vibrational, and electronic properties of glassy GeSe<sub>2</sub>, *Phys. Rev. B* 54 (1996) 12162–12171.
- [31] B. Bhattarai, D.A. Drabold, Vibrations in amorphous silica, *J. Non-Cryst. Solids* 439 (2016) 6–14.
- [32] S.M. Nakhmanson, D.A. Drabold, Approximate ab initio calculation of vibrational properties of hydrogenated amorphous silicon with inner voids, *Phys. Rev. B* 58 (1998) 15325–15328.
- [33] C.S. Casari, A.L. Bassi, A. Baserga, L. Ravagnan, P. Piseri, C. Lenardi, M. Tommasini, A. Milani, D. Fazzi, C.E. Bottani, P. Milani, Low-frequency modes in the Raman spectrum of sp<sup>2</sup>-nanostructured carbon, *Phys. Rev. B* 77 (2008), 195444(1–7).
- [34] W. Kamitakahara, J. Lannin, R. Cappelletti, J. Copley, F. Li, Vibrational spectroscopy of C<sub>60</sub> and graphitic carbons, *Phys. B* 180–181 (1992) 709–710.
- [35] Y. Takahashi, E.F. Westrum Jr., Glassy carbon low-temperature thermodynamic properties, *J. Chem. Thermodyn.* 2 (1970) 847–854.
- [36] A. Maradudin, E. Montroll, G.H. Weiss, *Theory of Lattice Dynamics in the Harmonic Approximation*, Academic Press, Newyork, 1963, p. 123.
- [37] J. Robertson, E. O'Reilly, Electronic and atomic structure of amorphous carbon, *Phys. Rev. B* 35 (1987) 2946–2957.
- [38] C. Chen, J. Robertson, Nature of disorder and localization in amorphous carbon, *J. Non-Cryst. Solids* 227–230 (1998) 602–606.
- [39] R.L. Cappelletti, M. Cobb, D.A. Drabold, W.A. Kamitakahara, Neutron scattering and ab initio molecular-dynamics study of vibrations in glassy GeSe<sub>2</sub>, *Phys. Rev. B* 52 (1995) 9133–9135.
- [40] A.D.W. Humphrey, K. Schulten, Vmd: visual molecular dynamics, *J. Mol. Graph.* 14 (1996) 33–38.